PARTICLE PHYSICS

High-precision measurement of the *W* boson mass with the CDF II detector

CDF Collaboration†‡, T. Aaltonen[1,2], S. Amerio[3,4], D. Amidei[5], A. Anastassov[6], A. Annovi[7], J. Antos[8,9], G. Apollinari[6], J. A. Appel[6], T. Arisawa[10], A. Artikov[11], J. Asaadi[12], W. Ashmanskas[6], B. Auerbach[13], A. Aurisano[12], F. Azfar[14], W. Badgett[6], T. Bae[15,16,17,18,19,20,21], A. Barbaro-Galtieri[22], V. E. Barnes[23], B. A. Barnett[24], P. Barria[25,26], P. Bartos[8,9], M. Bauce[3,4], F. Bedeschi[25], S. Behari[6], G. Bellettini[25,27], J. Bellinger[28], D. Benjamin[29], A. Beretvas[6], A. Bhatti[30], K. R. Bland[31], B. Blumenfeld[24], A. Bocci[29], A. Bodek[32], D. Bortoletto[23], J. Boudreau[33], A. Boveia[34], L. Brigliadori[35,36], C. Bromberg[37], E. Brucken[1,2], J. Budagov[11]§, H. S. Budd[32], K. Burkett[6], G. Busetto[3,4], P. Bussey[38], P. Butti[25,27], A. Buzatu[38], A. Calamba[39], S. Camarda[40], M. Campanelli[41], B. Carls[42], D. Carlsmith[28], R. Carosi[25], S. Carrillo[43]§, B. Casal[44], M. Casarsa[45], A. Castro[35,36], P. Catastini[46], D. Cauz[45,47,48], V. Cavaliere[42], A. Cerri[22], L. Cerrito[41], Y. C. Chen[49], M. Chertok[50], G. Chiarelli[25], G. Chlachidze[6], K. Cho[15,16,17,18,19,20,21], D. Chokheli[11], A. Clark[51], C. Clarke[52], M. E. Convery[6], J. Conway[50], M. Corbo[6], M. Cordelli[7], C. A. Cox[50], D. J. Cox[50], M. Cremonesi[25], D. Cruz[12], J. Cuevas[44], R. Culbertson[6], N. d'Ascenzo[6], M. Datta[6], P. de Barbaro[32], L. Demortier[30], M. Deninno[35]§, M. D'Errico[3,4], F. Devoto[1,2], A. Di Canto[25,27], B. Di Ruzza[6], J. R. Dittmann[31], S. Donati[25,27], M. D'Onofrio[53], M. Dorigo[45,54], A. Driutti[45,47,48], K. Ebina[10], R. Edgar[5], A. Elagin[34], R. Erbacher[50], S. Errede[42], B. Esham[42], S. Farrington[14], J. P. Fernández Ramos[55], R. Field[43], G. Flanagan[6], R. Forrest[50], M. Franklin[46], J. C. Freeman[6], H. Frisch[34], Y. Funakoshi[10], C. Galloni[25,27], A. F. Garfinkel[23], P. Garosi[25,26], H. Gerberich[42], E. Gerchtein[6], S. Giagu[56], V. Giakoumopoulou[57], K. Gibson[33], C. M. Ginsburg[6], N. Giokaris[57]§, P. Giromini[7], V. Glagolev[11], D. Glenzinski[6], M. Gold[58], D. Goldin[12], A. Golossanov[6], G. Gomez[44], G. Gomez-Ceballos[59], M. Goncharov[59], O. González López[55], I. Gorelov[58], A. T. Goshaw[29], K. Goulianos[30], E. Gramellini[35], C. Grosso-Pilcher[34], J. Guimaraes da Costa[46], S. R. Hahn[6], J. Y. Han[32], F. Happacher[7], K. Hara[60], M. Hare[61], R. F. Harr[52], T. Harrington-Taber[6], K. Hatakeyama[31], C. Hays[14], J. Heinrich[62], M. Herndon[28], A. Hocker[6], Z. Hong[12], W. Hopkins[6], S. Hou[49], R. E. Hughes[63], U. Husemann[64], M. Hussein[37], J. Huston[37], G. Introzzi[25,65,66], M. Iori[56,67], A. Ivanov[50], E. James[6], D. Jang[39], B. Jayatilaka[6], E. J. Jeon[15,16,17,18,19,20,21], S. Jindariani[6], M. Jones[23], K. K. Joo[15,16,17,18,19,20,21], S. Y. Jun[39], T. R. Junk[6], M. Kambeitz[68], T. Kamon[15,16,17,18,19,20,21,12], P. E. Karchin[52], A. Kasmi[31], Y. Kato[69], W. Ketchum[34], J. Keung[62], B. Kilminster[6], D. H. Kim[15,16,17,18,19,20,21], H. S. Kim[6], J. E. Kim[15,16,17,18,19,20,21], M. J. Kim[7], S. H. Kim[60], S. B. Kim[15,16,17,18,19,20,21], Y. J. Kim[15,16,17,18,19,20,21], Y. K. Kim[34], N. Kimura[10], M. Kirby[6], K. Kondo[10]§, D. J. Kong[15,16,17,18,19,20,21], J. Konigsberg[43], A. V. Kotwal[29]*, M. Kreps[68], J. Kroll[62], M. Kruse[29], T. Kuhr[68], M. Kurata[60], A. T. Laasanen[23], S. Lammel[6], M. Lancaster[41], K. Lannon[63], G. Latino[25,26], H. S. Lee[15,16,17,18,19,20,21], J. S. Lee[15,16,17,18,19,20,21], S. Leo[42], S. Leone[25], J. D. Lewis[6], A. Limosani[29], E. Lipeles[62], A. Lister[51], Q. Liu[23], T. Liu[6], S. Lockwitz[64], A. Loginov[64]§, D. Lucchesi[3,4], A. Lucà[7,6], J. Lueck[68], P. Lujan[22], P. Lukens[6], G. Lungu[30], J. Lys[22]§, R. Lysak[8,9], R. Madrak[6], P. Maestro[25,26], S. Malik[30], G. Manca[53], A. Manousakis-Katsikakis[57], L. Marchese[35], F. Margaroli[56], P. Marino[25,70], K. Matera[42], M. E. Mattson[52], A. Mazzacane[6], P. Mazzanti[35], R. McNulty[53], A. Mehta[53], P. Mehtala[1,2], A. Menzione[25]§, C. Mesropian[30], T. Miao[6], E. Michielin[3,4], D. Mietlicki[5], A. Mitra[49], H. Miyake[60], S. Moed[6], N. Moggi[35], C. S. Moon[15,16,17,18,19,20,21], R. Moore[6], M. J. Morello[25,70], A. Mukherjee[6], Th. Muller[68], P. Murat[6], M. Mussini[35,36], J. Nachtman[6], Y. Nagai[60], J. Naganoma[10], I. Nakano[71], A. Napier[61], J. Nett[12], T. Nigmanov[33], L. Nodulman[13], S. Y. Noh[15,16,17,18,19,20,21], O. Norniella[42], L. Oakes[14], S. H. Oh[29], Y. D. Oh[15,16,17,18,19,20,21], T. Okusawa[69], R. Orava[1,2], L. Ortolan[40], C. Pagliarone[45], E. Palencia[44], P. Palni[58], V. Papadimitriou[6], W. Parker[28], G. Pauletta[45,47,48], M. Paulini[39], C. Paus[59], T. J. Phillips[29], G. Piacentino[6], E. Pianori[62], J. Pilot[50], K. Pitts[42], C. Plager[72], L. Pondrom[28], S. Poprocki[6], K. Potamianos[22], A. Pranko[22], F. Prokoshin[11], F. Ptohos[7], G. Punzi[25,27], I. Redondo Fernández[55], P. Renton[14], M. Rescigno[56], F. Rimondi[35]§, L. Ristori[25,6], A. Robson[38], T. Rodriguez[62], S. Rolli[61], M. Ronzani[25,27], R. Roser[6], J. L. Rosner[34], F. Ruffini[25,26], A. Ruiz[44], J. Russ[39], V. Rusu[6], W. K. Sakumoto[32], Y. Sakurai[10], L. Santi[45,47,48], K. Sato[60], V. Saveliev[6], A. Savoy-Navarro[6], P. Schlabach[6], E. E. Schmidt[6], T. Schwarz[5], L. Scodellaro[44], F. Scuri[25], S. Seidel[58], Y. Seiya[69], A. Semenov[11], F. Sforza[25,27], S. Z. Shalhout[50], T. Shears[53], P. F. Shepard[33], M. Shimojima[60], M. Shochet[34], I. Shreyber-Tecker[73], A. Simonenko[11], K. Sliwa[61], J. R. Smith[50], F. D. Snider[6], H. Song[33], V. Sorin[40], R. St. Denis[38]§, M. Stancari[6], D. Stentz[6], J. Strologas[58], Y. Sudo[60], A. Sukhanov[6], I. Suslov[11], K. Takemasa[60], Y. Takeuchi[60], J. Tang[34], M. Tecchio[5], P. K. Teng[49], J. Thom[6], E. Thomson[62], V. Thukral[12], D. Toback[12], S. Tokar[8,9], K. Tollefson[37], T. Tomura[60], S. Torre[7], D. Torretta[6], P. Totaro[3], M. Trovato[25,70], F. Ukegawa[60], S. Uozumi[15,16,17,18,19,20,21], F. Vázquez[43], G. Velev[6], K. Vellidis[57], C. Vernieri[25,70], M. Vidal[23], R. Vilar[44], J. Vizán[44], G. Volpi[7], P. Wagner[62], R. Wallny[6], S. M. Wang[49], D. Waters[41], W. C. Wester III[6], D. Whiteson[62], A. B. Wicklund[13], S. Wilbur[50], H. H. Williams[62], J. S. Wilson[5], P. Wilson[6], B. L. Winer[63], P. Wittich[6], S. Wolbers[6], H. Wolfmeister[63], T. Wright[5], X. Wu[51], Z. Wu[31], K. Yamamoto[69], D. Yamato[69], T. Yang[6], U. K. Yang[15,16,17,18,19,20,21], Y. C. Yang[15,16,17,18,19,20,21], W.-M. Yao[22], G. P. Yeh[6], K. Yi[6], J. Yoh[6], K. Yorita[10], T. Yoshida[69], G. B. Yu[15,16,17,18,19,20,21], I. Yu[15,16,17,18,19,20,21], A. M. Zanetti[45], Y. Zeng[29], C. Zhou[29], S. Zucchelli[35,36]

The mass of the *W* boson, a mediator of the weak force between elementary particles, is tightly constrained by the symmetries of the standard model of particle physics. The Higgs boson was the last missing component of the model. After observation of the Higgs boson, a measurement of the *W* boson mass provides a stringent test of the model. We measure the *W* boson mass, M_W, using data corresponding to 8.8 inverse femtobarns of integrated luminosity collected in proton-antiproton collisions at a 1.96 tera–electron volt center-of-mass energy with the CDF II detector at the Fermilab Tevatron collider. A sample of approximately 4 million *W* boson candidates is used to obtain $M_W = 80,433.5 \pm 6.4_{\text{stat}} \pm 6.9_{\text{syst}} = 80,433.5 \pm 9.4$ MeV/c^2, the precision of which exceeds that of all previous measurements combined (stat, statistical uncertainty; syst, systematic uncertainty; MeV, mega–electron volts; *c*, speed of light in a vacuum). This measurement is in significant tension with the standard model expectation.

T he observation of the Higgs boson (*1–4*) at the Large Hadron Collider (LHC) (*5, 6*) has validated the last missing piece of the standard model (SM) (*7–9*) of elementary particle physics. This model, which incorporates quantum mechanics, special relativity, gauge symmetry, and group theory, currently describes most particle physics measurements with high accuracy. It postulates a number of experimentally established symmetries among particle properties, which tightly constrain the parameters of the model from experimental data (*10*). Given the current experimental precision and the predictive power of the SM, global fits of the model to the data render precise estimates of fundamental parameters, such as the mass of the *W* boson. As one of the mediators of the weak nuclear force, this particle is a key component of the SM framework. Its mass, one of the most important parameters in particle physics, is presently constrained by SM global fits to a relative precision of 0.01%, providing a strong motivation to test the SM by measuring the *W* boson mass to the same level of precision.
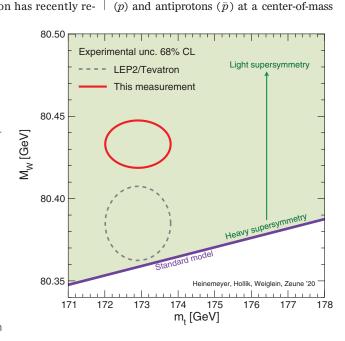
All fundamental particle masses, including that of the *W* boson, are generated in the SM through interactions with the condensate of the Higgs field in the vacuum. The formation of the condensate and the quantum excitation of this field, the Higgs boson (*2–4*), are parametrized but not explained by the SM. A number of hypotheses have been promulgated to provide a deeper explanation of the Higgs field, its potential, and the Higgs boson. These include supersymmetry—a spacetime symmetry relating fermions and bosons [[*11*] and references therein]—and compositeness, in which additional strong confining interactions produce the Higgs boson as a bound state [[*12*] and

references therein]. Many of these hypotheses include a source of dark matter, which is currently believed to comprise ~84% of the matter in the universe (10) but cannot be accounted for in the SM. Evidence for dark matter is provided by the abnormally high speeds of revolution of stars at large radii in galaxies, the velocities of galaxies in galaxy clusters, x-ray emissions sensing the temperature of hot gas in galaxy clusters, and the weak gravitational lensing of background galaxies by clusters [(13, 14) and references therein]. The additional symmetries and fields in these extensions to the SM would modify (15–24) the estimated mass of the W boson (Fig. 1) relative to the SM expectation (10) of $M_W = 80{,}357 \pm 4_{\text{inputs}} \pm 4_{\text{theory}}$ MeV (25). The SM expectation is derived from a combination of analytical relations from perturbative expansions on the basis of the internal symmetries of the theory and a set of high-precision measurements of observables, including the Z and Higgs boson masses, the top-quark mass, the electromagnetic (EM) coupling, and the muon lifetime, which are used as inputs to the analytical relations. The uncertainties in the SM expectation arise from uncertainties in the data-constrained input parameters (10) and from missing higher-order terms in the perturbative SM calculation (26, 27). An example of a nonsupersymmetric SM extension is a modified Higgs sector that includes an additional scalar field with no SM gauge interactions, which predicts an M_W shift of up to ~100 MeV (17), depending on the mass of the additional scalar particle and its interaction with the SM Higgs boson. A light (heavy) additional scalar particle would induce a positive (negative) M_W shift. Similar but smaller shifts of 20 to 40 MeV have been calculated in an extension that contains a second Higgs-like field with the same gauge charges as the SM Higgs field (18). Implications of very weakly interacting new particles such as "dark

photons" (19), restoration of parity conservation in the weak interaction (20), the possible composite nature of the Higgs boson (21), and model-independent modifications of the Higgs boson's interactions (22–24) have also been evaluated.

Previous analyses (28–44) yield a value of $M_W = 80{,}385 \pm 15$ MeV (45) from the combination of Large Electron-Positron (LEP) collider and Fermilab Tevatron collider measurements. The ATLAS Collaboration has recently re-

ported a measurement, $M_W = 80{,}370 \pm 19$ MeV (46, 47), that is comparable in precision to the Tevatron results. The LEP, Tevatron, and ATLAS measurements have not yet been combined, pending evaluation of uncertainty correlations.

CDF experiment at Tevatron

The Fermilab Tevatron produced high yields of W bosons from 2002 to 2011 through quark-antiquark annihilation in collisions of protons (p) and antiprotons ($\bar{p}$) at a center-of-mass

Fig. 1. Experimental measurements and theoretical predictions for the W boson mass. The red continuous ellipse shows the M_W measurement reported in this paper and the global combination of top-quark mass measurements, $m_t = 172.89 \pm 0.59$ GeV (10). The correlation between the M_W and m_t measurements is negligible. The gray dashed ellipse, updated (16) from (15), shows the 68% confidence level (CL) region allowed by the previous LEP-Tevatron combination $M_W = 80{,}385 \pm 15$ MeV (45) and m_t (10). That combination includes the M_W measurement published by CDF in 2012 (41, 43), which this

paper both updates (increasing M_W by 13.5 MeV) and subsumes. As an illustration, the green shaded region (15) shows the predicted mass of the W boson as a function of the top-quark mass m_t in the minimal supersymmetric extension (one of many possible extensions) of the standard model (SM), for a range of supersymmetry model parameters as described in (15). The thick purple line at the lower edge of the green region corresponds to the SM prediction with the Higgs boson mass measured at the LHC (10) used as input. The arrow indicates the variation of the predicted W boson mass as the mass scale of supersymmetric particles is lowered. The supersymmetry model parameter scan is for illustrative purposes and does not incorporate all exclusions from direct searches at the LHC. unc., uncertainty.

[1]Division of High Energy Physics, Department of Physics, University of Helsinki, FIN-00014, Helsinki, Finland. [2]Helsinki Institute of Physics, FIN-00014, Helsinki, Finland. [3]Istituto Nazionale di Fisica Nucleare, Sezione di Padova, I-35131 Padova, Italy. [4]University of Padova, I-35131 Padova, Italy. [5]University of Michigan, Ann Arbor, MI 48109, USA. [6]Fermi National Accelerator Laboratory, Batavia, IL 60510, USA. [7]Laboratori Nazionali di Frascati, Istituto Nazionale di Fisica Nucleare, I-00044 Frascati, Italy. [8]Comenius University, 842 48 Bratislava, Slovakia. [9]Institute of Experimental Physics, 040 01 Kosice, Slovakia. [10]Waseda University, Tokyo 169, Japan. [11]Joint Institute for Nuclear Research, Dubna RU-141980, Russia. [12]Mitchell Institute for Fundamental Physics and Astronomy, Texas A&M University, College Station, TX 77843, USA. [13]Argonne National Laboratory, Argonne, IL 60439, USA. [14]University of Oxford, Oxford OX1 3RH, UK. [15]Center for High Energy Physics, Kyungpook National University, Daegu 702-701, Korea. [16]Seoul National University, Seoul 151-742, Korea. [17]Sungkyunkwan University, Suwon 440-746, Korea. [18]Korea Institute of Science and Technology Information, Daejeon 305-806, Korea. [19]Chonnam National University, Gwangju 500-757, Korea. [20]Chonbuk National University, Jeonju 561-756, Korea. [21]Ewha Womans University, Seoul 120-750, Korea. [22]Ernest Orlando Lawrence Berkeley National Laboratory, Berkeley, CA 94720, USA. [23]Purdue University, West Lafayette, IN 47907, USA. [24]The Johns Hopkins University, Baltimore, MD 21218, USA. [25]Istituto Nazionale di Fisica Nucleare Pisa, I-56127 Pisa, Italy. [26]University of Siena, I-53100 Siena, Italy. [27]University of Pisa, I-56126 Pisa, Italy. [28]University of Wisconsin-Madison, Madison, WI 53706, USA. [29]Duke University, Durham, NC 27708, USA. [30]The Rockefeller University, New York, NY 10065, USA. [31]Baylor University, Waco, TX 76798, USA. [32]University of Rochester, Rochester, NY 14627, USA. [33]University of Pittsburgh, Pittsburgh, PA 15260, USA. [34]Enrico Fermi Institute, University of Chicago, Chicago, IL 60637, USA. [35]Istituto Nazionale di Fisica Nucleare Bologna, I-40127 Bologna, Italy. [36]University of Bologna, I-40127 Bologna, Italy. [37]Michigan State University, East Lansing, MI 48824, USA. [38]Glasgow University, Glasgow G12 8QQ, UK. [39]Carnegie Mellon University, Pittsburgh, PA 15213, USA. [40]Institut de Fisica d'Altes Energies, ICREA, Universitat Autonoma de Barcelona, E-08193 Bellaterra (Barcelona), Spain. [41]University College London, London WC1E 6BT, UK. [42]University of Illinois, Urbana, IL 61801, USA. [43]University of Florida, Gainesville, FL 32611, USA. [44]Instituto de Fisica de Cantabria, CSIC-University of Cantabria, 39005 Santander, Spain. [45]Istituto Nazionale di Fisica Nucleare Trieste, I-34127 Trieste, Italy. [46]Harvard University, Cambridge, MA 02138, USA. [47]Gruppo Collegato di Udine, I-33100 Udine, Italy. [48]Istituto Nazionale di Fisica Nucleare Udine, I-33100 Udine, Italy. [49]Institute of Physics, Academia Sinica, Taipei, Taiwan 11529, Republic of China. [50]University of California, Davis, Davis, CA 95616, USA. [51]University of Geneva, CH-1211 Geneva 4, Switzerland. [52]Wayne State University, Detroit, MI 48201, USA. [53]University of Liverpool, Liverpool L69 7ZE, UK. [54]University of Trieste, I-34127 Trieste, Italy. [55]Centro de Investigaciones Energeticas Medioambientales y Tecnologicas, E-28040 Madrid, Spain. [56]Istituto Nazionale di Fisica Nucleare, Sezione di Roma 1, I-00185 Roma, Italy. [57]National and Kapodistrian University of Athens, 157 71 Athens, Greece. [58]University of New Mexico, Albuquerque, NM 87131, USA. [59]Massachusetts Institute of Technology, Cambridge, MA 02139, USA. [60]University of Tsukuba, Tsukuba, Ibaraki 305, Japan. [61]Tufts University, Medford, MA 02155, USA. [62]University of Pennsylvania, Philadelphia, PA 19104, USA. [63]The Ohio State University, Columbus, OH 43210, USA. [64]Yale University, New Haven, CT 06520, USA. [65]Istituto Nazionale di Fisica Nucleare Pavia, I-27100 Pavia, Italy. [66]University of Pavia, I-27100 Pavia, Italy. [67]Sapienza Università di Roma, I-00185 Roma, Italy. [68]Institut für Experimentelle Kernphysik, Karlsruhe Institute of Technology, D-76131 Karlsruhe, Germany. [69]Osaka City University, Osaka 558-8585, Japan. [70]Scuola Normale Superiore, I-56126 Pisa, Italy. [71]Okayama University, Okayama 700-8530, Japan. [72]University of California, Los Angeles, Los Angeles, CA 90024, USA. [73]Institution for Theoretical and Experimental Physics, ITEP, Moscow 117259, Russia.
*Corresponding author. Email: ashutosh.kotwal@duke.edu
†All listed authors are members of the collaboration. ‡Visitors' institutions are listed in the supplementary materials. §Deceased.

energy of 1.96 TeV. The (anti)quark momentum distributions in the (anti)proton are the best-measured among all constituent partons of the colliding particles. The use of proton-antiproton collisions reduces uncertainties on the momenta of the partons and the corresponding M_W uncertainty relative to the LHC, where W bosons are produced from quarks or antiquarks and gluons, the latter of which have less precisely known momentum distributions. The moderate collision energy at the Tevatron further restricts the parton momenta to a range in which their distributions are known more precisely, compared with the relevant range at the LHC. The LHC detectors partially compensate with larger lepton rapidity coverage. The improved lepton resolution at the LHC detectors has a minor impact on the M_W uncertainty. Although the LHC dataset is much larger, the lower instantaneous luminosity at the Tevatron and in dedicated low-luminosity LHC runs helps to improve the resolution on certain kinematic quantities, compared with the typical LHC runs.

The data sample corresponds to an integrated luminosity of 8.8 inverse femtobarns (fb^{-1}) of $p\bar{p}$ collisions collected by the CDF II detector (43) between 2002 and 2011 and supersedes the earlier result obtained from a quarter of these data (41, 43). In this cylindrical detector [figure 3 of (43)], trajectories of charged particles (tracks) produced in the collisions are measured by means of a wire drift chamber (a central outer tracking drift chamber, or COT) (48) immersed in a 1.4-T axial magnetic field. Energy and position measurements of particles are also provided by EM and hadronic calorimeters surrounding the COT. The calorimeter elements have a projective tower geometry, with each tower pointing back to the average beam collision point at the center of the detector. Additional drift chambers (49) surrounding the calorimeters identify muon candidates as penetrating particles. The momentum perpendicular to the beam axis (cylindrical z axis) is denoted as p_T (if measured in the COT) or E_T (if measured in the calorimeters). The measurement uses high-purity samples of electron and muon (together referred to as lepton) decays of the $W^{\pm}$ bosons, $W \to e\nu$ and $W \to \mu\nu$, respectively (e, electron; ν, neutrino; μ, muon).

W and Z boson event selection

Events with a candidate muon with $p_T > 18$ GeV or electron with $E_T > 18$ GeV (50) are selected online by the trigger system for offline analysis. The following offline criteria select fairly pure samples of $W \to \mu\nu$ and $W \to e\nu$ decays. Muon candidates must have $p_T > 30$ GeV, with requirements on COT-track quality, calorimeter-energy deposition, and muon-chamber signals. Cosmic-ray muons are rejected with a targeted tracking algorithm (51). Electron candidates must have a COT track with $p_T > 18$ GeV and an EM calorimeter-energy deposition with $E_T > 30$ GeV and must meet requirements for COT track quality, matching of position and energy measured in the COT and in the calorimeter ($E_T/p_T < 1.6$), and spatial distributions of energy depositions in the calorimeters (43). Leptons are required to be central in pseudorapidity ($|\eta| < 1$) (50) and within the fiducial region where the relevant detector systems have high efficiency and uniform response. When selecting the W boson candidate sample, we suppress the Z boson background by rejecting events with a second lepton of the same flavor. Events that contain two oppositely charged leptons of the same flavor with invariant mass in the range of 66 to 116 GeV and with dilepton $p_T < 30$ GeV provide Z boson control samples ($Z \to ee$ and $Z \to \mu\mu$) to measure the detector response, resolution, and efficiency, as well as the boson p_T distributions. Details of the event selection criteria are described in (43).

The W boson mass is inferred from the kinematic distributions of the decay leptons (ℓ). Because the neutrino from the W boson decay is not directly detectable, its transverse momentum p_T^ν is deduced by imposing transverse momentum conservation. Longitudinal momentum balance cannot be imposed because most of the beam momenta are carried away by collision products that remain close to the beam axis, outside the instrumented regions of the detector. By design of the detector, such products have small transverse momentum. The transverse momentum vector sum of all detectable collision products accompanying the W or Z boson is defined as the hadronic recoil $\vec{u} = \Sigma_i E_i \sin(\theta_i)\hat{n}_i$, where the sum is performed over calorimeter towers (52) with energy E_i, polar angle θ_i, and transverse di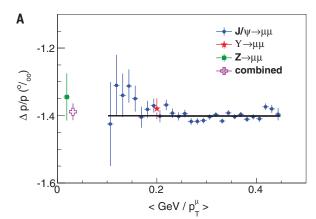rections specified by unit vectors $\hat{n}_i$. Calorimeter towers containing energy deposition from the charged lepton(s) are excluded from this sum. The transverse momentum vector of the neutrino $\vec{p}_T^\nu$ is inferred as $\vec{p}_T^\nu \equiv -\vec{p}_T^\ell - \vec{u}$ from $\vec{p}_T$ conservation, where $\vec{p}_T^\ell$ is the vector p_T (E_T) of the muon (electron). In analogy with a two-body mass, the W boson transverse mass is defined using only the transverse momentum vectors as $m_T = \sqrt{2\left(p_T^\ell p_T^\nu - \vec{p}_T^\ell \cdot \vec{p}_T^\nu\right)}$ (53). High-purity samples of W bosons are obtained with the requirements $30 < p_T^\ell < 55$ GeV, $30 < p_T^\nu < 55$ GeV, $|\vec{u}| < 15$ GeV, and $60 < m_T < 100$ GeV. This selection retains samples containing precise M_W information 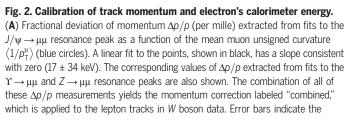and low backgrounds. The final samples of W and Z bosons consist of 1,811,700 (66,180) $W \to e\nu$ ($Z \to ee$) candidates and 2,424,486 (238,534) $W \to \mu\nu$ ($Z \to \mu\mu$) candidates.

Simulation of physical processes

The data distributions of m_T, p_T^ℓ, and p_T^ν are compared with corresponding simulated line shapes ("templates") as functions of M_W from a custom Monte Carlo simulation that has been designed and written for this analysis. A binned likelihood is maximized to obtain the mass and its statistical uncertainty. The kinematic properties of W and Z boson production and decay are simulated using the RESBOS program (54–56), which calculates the differential cross section with respect to boson mass, transverse momentum, and rapidity for boson production and decay. The calculation is performed at next-to-leading order in perturbative quantum chromodynamics (QCD), along with next-to-next-to-leading logarithm resummation of higher-order radiative quantum amplitudes. RESBOS offers one of the most accurate theoretical calculations available for these processes. The nonperturbative model parameters in RESBOS and the QCD interaction coupling strength α_s are external inputs needed to complete the description of the boson p_T spectrum and are constrained from the high-resolution dilepton $p_T^{\ell\ell}$ spectrum of the Z boson data and the p_T^W data spectrum. EM radiation from the leptons is modeled with the PHOTOS program (57), which is calibrated to the more accurate HORACE program (58, 59). We use the NNPDF3.1 (60) parton distribution functions (PDFs) of the (anti)proton, as they incorporate the most complete relevant datasets of the available next-to-next-to-leading order (NNLO) PDFs. Using 25 symmetric eigenvectors of the NNPDF3.1 set, we estimate a PDF uncertainty of 3.9 MeV. We find that the CT18 (61), MMHT2014 (62), and NNPDF3.1 NNLO PDF sets produce consistent results for the W boson mass, within ±2.1 MeV of the midpoint of the interval spanning the range of

Table 1. Individual fit results and uncertainties for the M_W measurements. The fit ranges are 65 to 90 GeV for the m_T fit and 32 to 48 GeV for the p_T^ℓ and p_T^ν fits. The χ^2 of the fit is computed from the expected statistical uncertainties on the data points. The bottom row shows the combination of the six fit results by means of the best linear unbiased estimator (66).

Distribution	W boson mass (MeV)	χ^2/dof
$m_T(e, \nu)$	$80{,}429.1 \pm 10.3_{stat} \pm 8.5_{syst}$	39/48
$p_T^\ell(e)$	$80{,}411.4 \pm 10.7_{stat} \pm 11.8_{syst}$	83/62
$p_T^\nu(e)$	$80{,}426.3 \pm 14.5_{stat} \pm 11.7_{syst}$	69/62
$m_T(\mu, \nu)$	$80{,}446.1 \pm 9.2_{stat} \pm 7.3_{syst}$	50/48
$p_T^\ell(\mu)$	$80{,}428.2 \pm 9.6_{stat} \pm 10.3_{syst}$	82/62
$p_T^\nu(\mu)$	$80{,}428.9 \pm 13.1_{stat} \pm 10.9_{syst}$	63/62
Combination	$80{,}433.5 \pm 6.4_{stat} \pm 6.9_{syst}$	7.4/5

Fig. 2. Calibration of track momentum and electron's calorimeter energy.
(**A**) Fractional deviation of momentum $\Delta p/p$ (per mille) extracted from fits to the $J/\psi \to \mu\mu$ resonance peak as a function of the mean muon unsigned curvature $\langle 1/p_T^{\mu} \rangle$ (blue circles). A linear fit to the points, shown in black, has a slope consistent with zero (17 ± 34 keV). The corresponding values of $\Delta p/p$ extracted from fits to the $\Upsilon \to \mu\mu$ and $Z \to \mu\mu$ resonance peaks are also shown. The combination of all of these $\Delta p/p$ measurements yields the momentum correction labeled "combined," which is applied to the lepton tracks in W boson data. Error bars indicate the

uncorrelated uncertainties (total uncertainty) for the individual boson measurements (combined correction). (**B**) Distribution of E/p for the $W \to e\nu$ data (points) and the best-fit simulation (histogram) including the small background from hadrons misreconstructed as electrons. The arrows indicate the fitting range used for the electron energy calibration. The relative energy correction ΔS_E, averaged over the calibrated W and Z boson data [see fig. S13 in (63)], is compatible with zero. In this and other figures, P_{KS} refers to the Kolmogorov-Smirnov probability of agreement between the shapes of the data and simulated distributions.

Fig. 3. Decay of the Z boson. (**A** and **B**) Distribution of (A) dimuon and (B) dielectron mass for candidate $Z \to \mu\mu$ and $Z \to ee$ decays, respectively. The data (points) are overlaid with the best-fit simulation template including the photon-mediated contribution (histogram). The arrows indicate the fitting range.

values. The model-dependent nature of the analysis implies that future improvements or corrections in any relevant theoretical modeling can be used to update our measurement quantifiably [see section IV of (63)].

The custom simulation includes a detailed calculation of the lepton and photon interactions in the detector (39, 43, 64), as well as models describing their individual position measurements within the COT. The COT position resolution as a function of radius is determined using muon tracks from Υ meson, W boson, and Z boson decays. All wire positions in the COT are measured with 1-μm precision using an in situ sample of cosmic ray muons (65), in addition to the electron tracks from W boson decays. The difference between electron and positron track momenta relative to their measured energy in the calorimeter (which

is independent of charge) strongly constrains certain modes of internal misalignment in the COT.

Momentum and energy calibration

The track momentum measurement in the COT is calibrated by measuring the masses of the J/ψ and $\Upsilon(1S)$ mesons reconstructed in their dimuon decays and comparing them with the known values (10). These meson mass measurements are performed with maximum-likelihood fits to the dimuon mass distributions from data, using templates obtained from the custom simulation. Measurements of these masses as functions of muon momenta are used to correct for small inaccuracies in the magnetic field map, the COT position measurements, and the modeling of the energy loss by particles traversing the detector. A

mismodeling of the energy loss would lead to a bias linear in the mean inverse p_T of the two muons. No such bias is observed after applying the magnetic field nonuniformity, COT, and energy-loss corrections (Fig. 2A). The curvature q/p_T measured by the COT, where q is the particle charge, is an analytic function of the true curvature. The curvature response function analytically yields a linear dependence of the measured invariant mass on p_T^{-1}, and higher-order terms in p_T^{-1} are negligible. The correction for the fractional deviation of the measured momentum from its correct value, $\Delta p/p \equiv p_{\text{measured}}/p_{\text{true}} - 1$, is inferred from the comparison of the measured meson masses to their more-precise world-average masses. The $\Delta p/p$ corrections extracted from the individual J/ψ and $\Upsilon(1S)$ invariant mass fits are consistent with each other, and the results
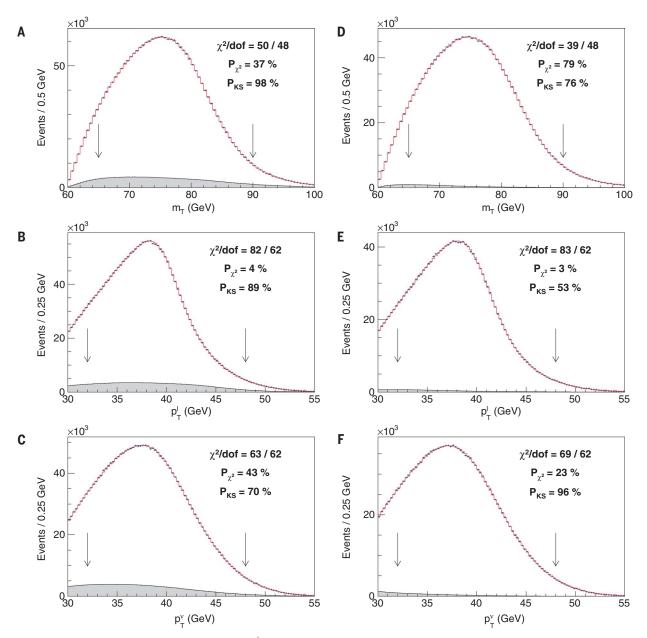
Fig. 4. Decay of the W boson. (A to C) Distributions for m_T (A), p_T^ℓ (B), and p_T^ν (C) for the muon channel. (**D to F**) Same as in (A) to (C) but for the electron channel. The data (points) and the best-fit simulation template (histogram) including backgrounds (shaded regions) are shown. The arrows indicate the fitting range.

are combined to obtain $\Delta p/p = (-1393 \pm 26)$ parts per million (ppm).

The combined momentum calibration is used to measure the Z boson mass in the dimuon channel (Fig. 3A), which is blinded with a random offset in the range of −50 to 50 MeV until all analysis procedures are established. The unblinded measurement is $M_Z = 91{,}192.0 \pm 6.4_{stat} \pm 4.0_{syst}$ MeV (stat, statistical uncertainty; syst, systematic uncertainty), which is consistent with the world average of $91{,}187.6 \pm 2.1$ MeV (10, 44) and therefore provides a precise consistency check. Systematic uncertainties on M_Z result from uncertainties on the longitudinal coordinate measurements in the COT (1.0 MeV), the momentum calibration (2.3 MeV), and the

QED radiative corrections (3.1 MeV). The latter two sources are correlated with the M_W measurement. The $Z \to \mu\mu$ mass measurement is then included in the final momentum calibration. The systematic uncertainties stemming from the magnetic field nonuniformity dominate the total uncertainty of 25 ppm in the combined momentum calibration.

After track momentum (p) calibration, the electron's calorimeter energy (E) is calibrated using the peak of the E/p distribution in $W \to e\nu$ (Fig. 2B) and $Z \to ee$ [fig. S13 in (63)] data. Fits to this peak in bins of electron E_T determine the electron energy calibration and its dependence on E_T. The radiative region of the E/p distribution ($E/p > 1.12$) is fitted to

measure a small correction (≈5%) to the amount of radiative material traversed in the tracking volume. The EM calorimeter resolution is measured using the widths of the E/p peak in the $W \to e\nu$ sample and of the mass peak of the $Z \to ee$ sample.

We use the calibrated electron energies to measure the Z boson mass in the dielectron channel (Fig. 3B), which is also blinded with the same offset as used for the dimuon channel. The unblinded result, $M_Z = 91{,}194.3 \pm 13.8_{stat} \pm 7.6_{syst}$ MeV, is consistent with the world average, providing a stringent consistency check of the electron energy calibration. Systematic uncertainties on M_Z are caused by uncertainties on the calorimeter energy

Fig. 5. Comparison of this CDF II measurement and past M_W measurements with the SM expectation. The latter includes the published estimates of the uncertainty (4 MeV) due to missing higher-order quantum corrections, as well as the uncertainty (4 MeV) from other global measurements used as input to the calculation, such as m_t. c, speed of light in a vacuum.

	W boson mass (MeV/c²)	
D0 I	80478 ± 83	
CDF I	80432 ± 79	
DELPHI	80336 ± 67	
L3	80270 ± 55	
OPAL	80415 ± 52	
ALEPH	80440 ± 51	
D0 II	80376 ± 23	
ATLAS	80370 ± 19	
CDF II	80433 ± 9	

(6.5 MeV) and track momentum (2.3 MeV), on the z coordinate measured in the COT (0.8 MeV), and on QED radiative corrections (3.1 MeV). Measurements of the Z boson mass using the dielectron track momenta, and comparisons of mass measurements using radiative and nonradiative electrons, provide consistent results. The final calibration of the electron energy is obtained by combining the E/p-based calibration with the $Z(\rightarrow ee)$ mass-based calibration, taking into account the correlated uncertainty on the radiative corrections.

The spectator partons in the proton and antiproton, as well as the additional (≈ 3) $p\bar{p}$ interactions in the same collider bunch crossing, contribute visible energy that degrades the resolution of $\vec{u}$. These contributions are measured from events triggered on inelastic $p\bar{p}$ interactions and random bunch crossings, reproducing the collision environment of the W and Z boson data. Because there are no high-p_T neutrinos in the Z boson data, the $\vec{p}_T^{\ell\ell}$ imbalance between the $\vec{p}_T^{\ell\ell}$ and $\vec{u}$ in $Z \rightarrow \ell\ell$ events is used to measure the calorimeter response to, and resolution of, the initial-state QCD radiation accompanying boson production. The simulation of the recoil vector $\vec{u}$ also requires knowledge of the distribution of the energy flow into the calorimeter towers impacted by the leptons, because these towers are excluded from the computation of $\vec{u}$. This energy flow is measured from the W boson data using the event-averaged response of towers separated in azimuth from the lepton direction.

Extracting the W boson mass

Kinematic distributions of background events passing the event selection are included in the template fits with their estimated normalizations. The W boson samples contain a small contamination of background events arising from QCD jet production with a hadron misidentified as a lepton, $Z \rightarrow \ell\ell$ decays with only one reconstructed lepton, $W \rightarrow \tau\nu \rightarrow \ell\nu\bar{\nu}\nu$, pion and kaon decays in flight to muons (DIF), and cosmic-ray muons (τ, tau lepton; $\bar{\nu}$, antineutrino). The jet, DIF, and cosmic-ray backgrounds are estimated from control samples of data, whereas the $Z \rightarrow \ell\ell$ and $W \rightarrow \tau\nu$ backgrounds are estimated from simulation. Background fractions for the muon (electron) datasets are evaluated to be 7.37% (0.14%) from $Z \rightarrow \ell\ell$ decays, 0.88% (0.94%) from $W \rightarrow \tau\nu$ decays, 0.01% (0.34%) from jets, 0.20% from DIF, and 0.01% from cosmic rays.

The fit results (Fig. 4) are summarized in Table 1. The M_W fit values are blinded during analysis with an unknown additive offset in the range of −50 to 50 MeV, in the same manner as, but independent of, the value used for blinding the Z boson mass fits. As the fits to the different kinematic variables have different sensitivities to systematic uncertainties, their consistency confirms that the sources of systematic uncertainties are well understood. Systematic uncertainties, propagated by varying the simulation parameters within their uncertainties and repeating the fits to these simulated data, are shown in Table 1. The correlated uncertainty in the m_T (p_T^ℓ, p_T^ν) fit between the muon and

electron channels is 5.8 (7.9, 7.4) MeV. The mass fits are stable with respect to variations of the fitting ranges.

Simulated experiments are used to evaluate the statistical correlations between fits, which are found to be 69% (68%) between m_T and p_T^ℓ (p_T^ν) fit results and 28% between p_T^ℓ and p_T^ν fit results (43). The six individual M_W results are combined (including correlations) by means of the best linear unbiased estimator (66) to obtain $M_W = 80{,}433.5 \pm 9.4$ MeV, with $\chi^2/\text{dof} = 7.4/5$ corresponding to a probability of 20%. The m_T, p_T^ℓ, and p_T^ν fits in the electron (muon) channel contribute weights of 30.0% (34.2%), 6.7% (18.7%), and 0.9% (9.5%), respectively. The combined result is shown in Fig. 1, and its associated systematic uncertainties are shown in Table 2.

Discussion

The dataset used in this analysis is about four times as large as the one used in the previous analysis (41, 43). Although the resolution of the hadronic recoil is somewhat degraded in the new data because of the higher instantaneous luminosity, the statistical precision of the measurement from the larger sample is still improved by almost a factor of 2. To achieve a commensurate reduction in systematic uncertainties, a number of analysis improvements have been incorporated, as described in table S1. These improvements are based on using cosmic-ray and collider data in ways not employed previously to improve (i) the COT alignment and drift model and the uniformity of the EM calorimeter response, and (ii) the accuracy and robustness of the detector response and resolution model in the simulation. Additionally, theoretical inputs to the analysis have been updated. Upon incorporating the improved understanding of PDFs and track reconstruction, our previous measurement is increased by 13.5 MeV to 80,400.5 MeV; the consistency of the latter with the new measurement is at the percent probability level.

In conclusion, we report a new measurement of the W boson mass with the complete dataset collected by the CDF II detector at the Fermilab Tevatron, corresponding to 8.8 fb^{-1} of integrated luminosity. This measurement, $M_W = 80{,}433.5 \pm 9.4$ MeV, is more precise than all previous measurements of M_W combined and subsumes all previous CDF measurements from 1.96-TeV data (38, 39, 41, 43). A comparison with the SM expectation of $M_W = 80{,}357 \pm 6$ MeV (10), treating the quoted uncertainties as independent, yields a difference with a significance of 7.0σ and suggests the possibility of improvements to the SM calculation or of extensions to the SM. This comparison, along with past measurements, is shown in Fig. 5. Using the method described in (45), we obtain a combined Tevatron (CDF and D0) result of $M_W = 80{,}427.4 \pm 8.9$ MeV. Assuming no correlation between the Tevatron

Table 2. Uncertainties on the combined M_W result.

Source	Uncertainty (MeV)
Lepton energy scale	3.0
Lepton energy resolution	1.2
Recoil energy scale	1.2
Recoil energy resolution	1.8
Lepton efficiency	0.4
Lepton removal	1.2
Backgrounds	3.3
p_T^Z model	1.8
p_T^W/p_T^Z model	1.3
Parton distributions	3.9
QED radiation	2.7
W boson statistics	6.4
Total	9.4

and LEP measurements, their average becomes $M_W = 80{,}424.2 \pm 8.7$ MeV.

REFERENCES AND NOTES

1. P. W. Anderson, *Phys. Rev.* **130**, 439–442 (1963).
2. F. Englert, R. Brout, *Phys. Rev. Lett.* **13**, 321–323 (1964).
3. P. W. Higgs, *Phys. Rev. Lett.* **13**, 508–509 (1964).
4. G. S. Guralnik, C. R. Hagen, T. W. B. Kibble, *Phys. Rev. Lett.* **13**, 585–587 (1964).
5. G. Aad et al.; ATLAS Collaboration, *Phys. Lett. B* **716**, 1–29 (2012).
6. S. Chatrchyan et al.; CMS Collaboration, *Phys. Lett. B* **716**, 30–61 (2012).
7. S. Glashow, *Nucl. Phys.* **22**, 579–588 (1961).
8. A. Salam, J. C. Ward, *Phys. Lett.* **13**, 168–171 (1964).
9. S. Weinberg, *Phys. Rev. Lett.* **19**, 1264–1266 (1967).
10. P. A. Zyla et al., *Prog. Theor. Exp. Phys.* **2020**, 083C01 (2020).
11. J. Feng, *Annu. Rev. Nucl. Part. Sci.* **63**, 351–382 (2013).
12. R. Contino, T. Krämer, M. Son, R. Sundrum, *J. High Energy Phys.* **2007**, 074 (2007).
13. G. Bertone, D. Hooper, J. Silk, *Phys. Rep.* **405**, 279–390 (2005).
14. J. L. Feng, *Annu. Rev. Astron. Astrophys.* **48**, 495–545 (2010).
15. S. Heinemeyer, W. Hollik, G. Weiglein, L. Zeune, *J. High Energy Phys.* **2013**, 84 (2013).
16. S. Heinemeyer, "Electroweak precision observables and BSM physics," presented at the Snowmass EF04 meeting, 17 July 2020; https://indico.fnal.gov/event/43577/contributions/191539/attachments/131503/161060/sven.pdf.
17. D. López-Val, T. Robens, *Phys. Rev. D* **90**, 114018 (2014).
18. D. López-Val, J. Sola, *Eur. Phys. J. C* **73**, 2393 (2013).
19. D. Curtin, R. Essig, S. Gori, J. Shelton, *J. High Energy Phys.* **2015**, 157 (2015).
20. J. Chakrabortty, J. Gluza, R. Sevillano, R. Szafron, *J. High Energy Phys.* **2012**, 38 (2012).
21. B. Bellazzini, C. Csáki, J. Serra, *Eur. Phys. J. C* **74**, 2766 (2014).
22. A. Pomarol, F. Riva, *J. High Energy Phys.* **2014**, 151 (2014).
23. G. F. Giudice, C. Grojean, A. Pomarol, R. Rattazzi, *J. High Energy Phys.* **2007**, 045 (2007).
24. S. F. Ge, H. J. He, R. Q. Xiao, *J. High Energy Phys.* **2016**, 7 (2016).
25. We use the convention $\hbar = c \equiv 1$ throughout this paper.
26. M. Awramik, M. Czakon, A. Freitas, G. Weiglein, *Phys. Rev. D* **69**, 053006 (2004).
27. J. Erler, M. Schott, *Prog. Part. Nucl. Phys.* **106**, 68–119 (2019).
28. T. Affolder et al.; CDF Collaboration, *Phys. Rev. D* **64**, 052001 (2001).
29. B. Abbott et al.; D0 Collaboration, *Phys. Rev. D* **58**, 092003 (1998).
30. B. Abbott et al.; D0 Collaboration, *Phys. Rev. Lett.* **84**, 222–227 (2000).
31. B. Abbott et al.; D0 Collaboration, *Phys. Rev. D* **62**, 092006 (2000).
32. V. M. Abazov et al.; D0 Collaboration, *Phys. Rev. D* **66**, 012001 (2002).
33. V. M. Abazov et al.; CDF Collaboration, D0 Collaboration, *Phys. Rev. D* **70**, 092008 (2004).
34. S. Schael et al.; ALEPH Collaboration, *Eur. Phys. J. C* **47**, 309–335 (2006).
35. J. Abdallah et al.; DELPHI Collaboration, *Eur. Phys. J. C* **55**, 1 (2008).
36. P. Achard et al.; L3 Collaboration, *Eur. Phys. J. C* **45**, 569–587 (2006).
37. G. Abbiendi et al.; OPAL Collaboration, *Eur. Phys. J. C* **45**, 307–335 (2006).
38. T. Aaltonen et al.; CDF Collaboration, *Phys. Rev. Lett.* **99**, 151801 (2007).
39. T. Aaltonen et al.; CDF Collaboration, *Phys. Rev. D* **77**, 112001 (2008).
40. V. M. Abazov et al.; D0 Collaboration, *Phys. Rev. Lett.* **103**, 141801 (2009).
41. T. Aaltonen et al.; CDF Collaboration, *Phys. Rev. Lett.* **108**, 151803 (2012).
42. V. M. Abazov et al.; D0 Collaboration, *Phys. Rev. Lett.* **108**, 151804 (2012).
43. T. Aaltonen et al.; CDF Collaboration, *Phys. Rev. D* **89**, 072003 (2014).
44. ALEPH Collaboration, CDF Collaboration, D0 Collaboration, DELPHI Collaboration, L3 Collaboration, OPAL Collaboration, SLD Collaboration, LEP Electroweak Working Group, Tevatron Electroweak Working Group, SLD electroweak heavy flavour groups, arXiv:1012.2367 [hep-ex] (2010) and references therein.
45. T. Aaltonen et al.; CDF Collaboration, D0 Collaboration, *Phys. Rev. D* **88**, 052018 (2013).
46. M. Aaboud et al.; ATLAS Collaboration, *Eur. Phys. J. C* **78**, 110 (2018).
47. M. Aaboud et al.; ATLAS Collaboration, *Eur. Phys. J. C* **78**, 898 (2018).
48. T. Affolder et al., *Nucl. Instrum. Methods Phys. Res. A* **526**, 249–299 (2004).
49. G. Ascoli et al., *Nucl. Instrum. Methods Phys. Res. A* **268**, 33–40 (1988).
50. The CDF II detector is centered on the beam (z) axis, which points in the proton direction. The $+x$ axis points outward and the $+y$ axis points upward, respectively, from the Tevatron ring. Corresponding cylindrical coordinates are defined with $r \equiv \sqrt{x^2 + y^2}$ and azimuthal angle $\phi \equiv \tan^{-1}(y/x)$. Pseudorapidity is defined as $\eta = -\ln[\tan(\theta/2)]$, where θ is the polar angle from the z axis. Energy (momentum) transverse to the beam is denoted as E_T (p_T).
51. A. V. Kotwal, H. K. Gerberich, C. Hays, *Nucl. Instrum. Methods Phys. Res. A* **506**, 110–118 (2003).
52. F. Abe et al.; CDF Collaboration, *Nucl. Instrum. Methods Phys. Res. A* **271**, 387 (1988).
53. J. Smith, W. L. van Neerven, J. A. M. Vermaseren, *Phys. Rev. Lett.* **50**, 1738–1740 (1983).
54. C. Balázs, C.-P. Yuan, *Phys. Rev. D* **56**, 5558–5583 (1997).
55. G. A. Ladinsky, C. Yuan, *Phys. Rev. D* **50**, R4239–R4243 (1994).
56. F. Landry, R. Brock, P. M. Nadolsky, C.-P. Yuan, *Phys. Rev. D* **67**, 073016 (2003).
57. P. Golonka, Z. Was, *Eur. Phys. J. C* **45**, 97–107 (2006).
58. C. M. Carloni Calame, G. Montagna, O. Nicrosini, A. Vicini, *J. High Energy Phys.* **2007**, 109 (2007).
59. A. V. Kotwal, B. Jayatilaka, *Adv. High Energy Phys.* **2016**, 1615081 (2016).
60. R. D. Ball et al., *Eur. Phys. J. C* **77**, 663 (2017).
61. T. J. Hou et al., *Phys. Rev. D* **103**, 014013 (2021).
62. L. A. Harland-Lang, A. D. Martin, P. Motylinski, R. S. Thorne, *Eur. Phys. J. C* **75**, 204 (2015).
63. Supplementary materials.
64. A. V. Kotwal, C. Hays, *Nucl. Instrum. Methods Phys. Res. A* **729**, 25–35 (2013).
65. A. V. Kotwal, C. Hays, *Nucl. Instrum. Methods Phys. Res. A* **762**, 85–99 (2014).
66. L. Lyons, D. Gibaut, P. Clifford, *Nucl. Instrum. Methods Phys. Res. A* **270**, 110–117 (1988).
67. T. Aaltonen et al. (CDF Collaboration), High precision measurement of the W-boson mass with the CDF II detector, Zenodo (2022); https://doi.org/10.5281/zenodo.6245867.

SUPPLEMENTARY MATERIALS

science.org/doi/10.1126/science.abk1781
Authors and Affiliations
Supplementary Text
Figs. S1 to S41
Tables S1 to S10
References (*68–110*)

27 June 2021; accepted 11 March 2022
10.1126/science.abk1781